Author's Accepted Manuscript

www.elsevier.com/locate/talanta

Affinity capture surface carboxyl-functionalized MoS2 sheets to enhance the sensitivity of surface plasmon resonance immunosensors

Nan-Fu Chiu, Ting-Li Lin

PII: S0039-9140(18)30313-8
DOI: https://doi.org/10.1016/j.talanta.2018.03.073
Reference: TAL18507

To appear in: *Talanta*

Received date: 16 January 2018
Revised date: 23 March 2018
Accepted date: 24 March 2018

Cite this article as: Nan-Fu Chiu and Ting-Li Lin, Affinity capture surface carboxyl-functionalized MoS2 sheets to enhance the sensitivity of surface plasmon resonance immunosensors, *Talanta,* https://doi.org/10.1016/j.talanta.2018.03.073

Affinity capture surface carboxyl-functionalized MoS2 sheets to enhance the sensitivity of surface plasmon resonance immunosensors

Nan-Fu Chiu*, Ting-Li Lin

Laboratory of Nano-photonics and Biosensors, Institute of Electro-Optical Science and Technology, National Taiwan Normal University, No. 88, Sec. 4, Ting-Chou Road, Taipei 11677, Taiwan

***Corresponding author:** TEL:+886-77346722 and Fax:+886-2-86631954, No. 88, Sec. 4, Ting-Chou Road, Taipei 11677, Taiwan. E-mail: nfchiu@ntnu.edu.tw

Abstract

The development of functionalized molybdenum disulfide (MoS_2) has led to a new trend in the biosensing field, owing to its high sensitivity and bio-affinity characteristics with regards to the simple synthesis of carboxyl-functionalized MoS_2 nanocomposites. In this study, we used monochloroacetic acid (MCA) to successfully modify carboxyl-MoS_2. The efficiency of this MCA modification method showed a higher -COOH group content of 30.1%, mainly due to chlorine atoms occupying the MoS2 sulfur vacancy to allow for the formation of a strong bonding effect. This then enhanced the surface area of -COOH and improved the formation of covalent bonds between proteins. We demonstrated that MoS_2-COOH-based surface plasmon resonance (SPR) chips can provide excellent sensitivity and high affinity for immunoassay biomolecules detected in a low sample volume of 20 μl. With respect to the shifts of the SPR angles of the chips, the high binding affinity at a BSA concentration of 14.5 nM for a MoS_2-COOH chip, a MoS_2 chip and a traditional SPR chip are 4.69 m^o, 2.49 m^o and 1.53 m^o, respectively. In addition, the MoS_2-COOH chip could amplify the SPR angle response by 3.1 folds and enhance the high association rate of ka by 212 folds compared to MoS_2 and traditional SPR chips. The results thus obtained revealed that the overall affinity binding value, K_A, of the MoS_2-COOH chip can be significantly enhanced by

up to ~6.5 folds that of the MoS_2 chip. In summary, the excellent binding affinity, biocompatible and high sensitivity suggest the potential of the clinical application of this MoS_2-COOH-based SPR chip detection method for *in vitro* diagnostic and point-of-care testing devices.

Graphical Abstract

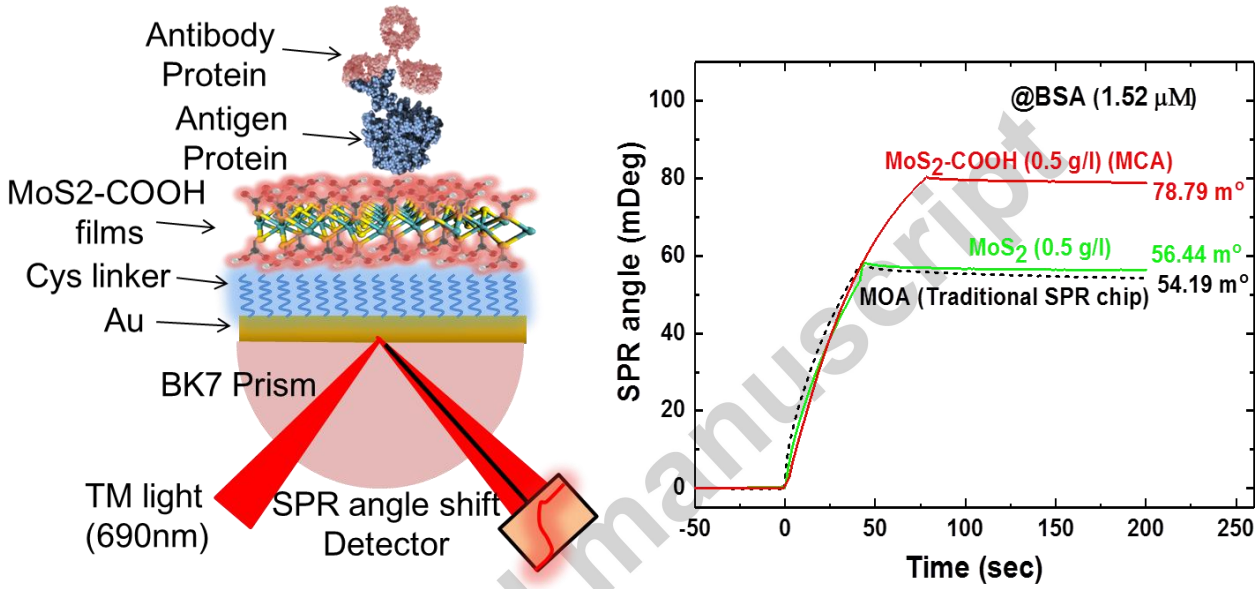

keywords: molybdenum disulfide (MoS_2), carboxyl-functionalized, bovine serum albumin (BSA), surface plasmon resonance (SPR), biosensor.

1. Introduction

Extremely thin two-dimensional layered materials (2DLMs) have attracted increasing attention due to their excellent electronic carrier mobility properties, exceptional tension and flexibility properties, and unique optical transparency, which are not readily achievable in other semiconductor nanostructures. 2DLMs such as graphene allotropes and transition metal dichalcogenides (TMDs) are set to revolutionize the industrial applications [1-3]. Furthermore, 2DLMs generated chemically and those synthesized via self-assembly of

organic molecules may be combined to create heterostructures or nanocomposites to form complex and totally new functional materials. Monolayers of TMD crystals (TMDCs) such as molybdenum disulfide (MoS_2), tungsten disulfide (WS_2), hexagonal molybdenum diselenide ($MoSe_2$), tungsten diselenide (WSe_2), and molybdenum ditelluride ($MoTe_2$) are semiconductors that form layered structures surrounded by a plane of hexagonal metal atoms have received special attention [4, 5]. These monolayers of semiconducting TMDCs have similar characteristics including 6 ~ 7 Å thickness, direct band gap and tunability of the energy gap, and they have been widely used in field effect transistors [1, 6-9], light emitting diodes [1, 10], solar cells [11-13], and sensors [14,15].These semiconducting TMDs have been extensively fabricated and studied, however metallic TMDs have recently received increasing attention, possibly due to plasmon-induced hot carrier science and technology issues [16, 17].

The plasmon mode of metallic TMDs exhibits a remarkable dynamical charge response, charge-density wave (CDW) [18], superconductivity [19, 20], and a clear effect of the crystal local-field impact [21]. The optical properties of metallic TMDCs are mainly controlled by plasmon excitation. Moreover the generation of metallic TMDCs is similar to graphene using doping or synthesis via self-assembly of organic molecules, and this constitutes a natural way of pushing the surface plasmon (SP) mode further toward the vis-NIR using a scalable bottom-up approach [22, 23].

MoS_2 is composed of many stacked S-Mo-S layers held together by van der Waals forces [22, 24, 25], which have much higher charge carrier densities leading to π and $\pi+\sigma$ SP modes at 6.5-7.6 eV and 15.6-20 eV [26, 27], which are substantially red-shifted [28, 29]. MoS_2 is similar to graphene in that it is not affected by dilute acid or oxygen, and it is unreactive with other chemicals. It also has the unique characteristics of electrical and photo-responsiveness of Shockley-type surface state properties. Therefore, MoS_2 has been widely studied with regards to SP enhanced photoluminescence (PL) [22, 28-30], energy

dispersion [30, 31], integrated circuits [32], photosensitivity [33], and highly efficient emitter [22, 34].

Recently, the use of MoS_2 in the biomedical sensing field has been widely discussed [35-39], however only with regards to surface plasmon resonance (SPR) sensing mechanism preliminary simulation analysis [40-42], and no experimental confirmation of the feasibility of the sensing mechanism has yet been reported. In this study, we propose a novel modification of a carboxyl-functionalized MoS_2 (MoS_2-COOH) nanocomposite for carboxylation techniques of monochloroacetic acid (MCA) on the surface. In carboxylation techniques, -COOH can improve charge carrier transfer, improve conductivity [43], and increase chain flexibility [44]. Therefore, the conductivity of 2D materials can be enhanced through the modification of -COOH to significantly enhance the conductivity and the resonant propagation characteristics of the plasmon [45]. The use of MCA to modify carboxyl-MoS_2 has not previously been reported, and to the first of our knowledge, this is the first experimental study to investigate the MoS_2-COOH-based SPR biosensing mechanism. We modified the SPR fluidic system requires only 20 μl analyte volumes for the immunoassay, and real-time molecule-molecule interactions and affinity kinetics analysis. The carboxyl group facilitated the resonance state modulation of the SP modes, improved the bio-affinity of the interface, and enhanced the sensitivity of the biosensing.

2. Experimental section

2.1 Synthesis of carboxyl-functionalized MoS_2 nanocomposite

2.1.1 Modification of MoS_2-COOH by monochloroacetic acid (MCA) synthesis:

MoS_2 (molybdenum IV sulfide) powder (99%, sheet size < 2 μm) was purchased from Sigma-Aldrich. We used a total of 15 ml of MoS_2 solution at a concentration of 2 mg/ml prepared using deionized water. After 1.2 g of sodium hydroxide (NaOH) and 1.0 g of monochloroacetic acid (MCA) were added to the MoS_2 solution, it was shaken using

ultrasound for 3 hours. According to the relevant literature, the use of ultrasonic shock waves will lead to vacancies in the surface of MoS_2 [46]. After homogeneous mixing, centrifugation was performed several times and the supernatant was replaced with deionized water. A monochloroacetic acid-modified carboxyl MoS_2 aqueous solution, called MoS_2-COOH (MCA), was prepared as shown in Figure 1(a). In the MCA modification mechanism, chlorine atoms occupied the sulfur vacancies rather than adhere to the surface [47].

2.2 Preparation of sensing films and protein immobilization method

The sensing chip was fabricated using a 0.17-mm thick BK7 coverslip substrate consisting of a 2-nm chromium (Cr) and 47-nm gold (Au) thin film deposited by thermal deposition as shown in Figure 1(b). The sensing film was chemically modified using thiol- and amine-group self-assembled monolayers (SAMs) of cystamine (Cys) (cystamine dihydrochloride 98%, Alfa Aesar, Ward Hill, MA, USA) to bridge MoS_2-COOH sheets of 1 g/l concentration on a 47-nm Au film. The Cys solution used double-distilled water (ddH_2O) diluted to 10 mM with an Au electrode immersed at room temperature for 24 hours. The carboxyl-functionalized MoS_2 sheets were immobilized on the surface of an Au/Cys electrode by strongly covalent bond reactions. The Au/Cys/MoS_2-COOH film was generated by using Au/Cys film immersed in aqueous MoS_2-COOH sheets for 5 hours, followed by thorough rinsing with deionized water to remove unbonded MoS_2-COOH.

Bovine serum albumin (BSA) was immobilized on the Au/Cys/MoS_2-COOH film, which activated the -COOH terminal group for a better affinity reaction and was beneficial for the amine (-NH_2) bonds of the protein to form strong chemical covalent bonds. The activation used 0.1 M N-hydroxysuccinimide (NHS) and 0.4 M l-ethyl-3-(3-dimethyl aminopropyl) carbodiimide (EDC) at a 1:1 volume ratio. The EDC/NHS solution was injected with a volume of 20 μl and flow rate of 6 μl/minute to activate the -COOH surface at room

temperature. This was immediately followed by the injection of BSA using the same volume of 20 µl and flow rate of 6 µl/minute to allow for immobilization on the MoS_2-COOH surface. Finally, a saturation concentration of 1 M ethanolamine (EA) solution was used on the sensing chip surface of all carboxylic groups as a blocking agent. The MoS_2-COOH-based SPR immunosensors are shown in Figure 1(c).

2.3 Preparation of a traditional Au-based SPR chip and protein immobilization method

A traditional SPR chip using 8-mercaptooctanoic acid (MOA; Sigma-Aldrich) on a modified Au surface was created by immersing an Au electrode into a solution of MOA (1 mM) for 24 hours at room temperature. MOA binds to the Au surface through a thiol linker (-SH end) resulting in monolayers which are terminated with carboxylic acid. The other steps were the same as with MoS_2-COOH for all immobilization procedures, and the injections of EDC/NHS, BSA and EA used the same volume of 20 µl and flow rate of 6 µl/minute. All SPR biosensors were calibrated via a standardized 60 m° with 1% ethanol solution using the volume of 20 µl and flow rate of 6 µl/minute in a SPR BI-3000 system (Biosensing Instrument, Tempe, AZ).

3. Results and Discussion

3.1 Analysis of morphology and spectral characteristics of modification

Figures 2(a) and 2(b) show transmission electron microscopy (TEM) images of MoS_2 and MoS_2-COOH sheets. The structural properties with the mixed SAM coated on the sensing chip were randomly arranged, and the layered structure was made from MoS_2 flakes. Figure 2(b) shows a change in the edge of the MoS_2 sheet modified by carboxylation. This phenomenon was caused by carboxylic acid, so that the MoS_2 surface became an organic chitosan matrix with a hydrophilic functional group [48].

The UV-visible absorption spectral properties of typical MoS_2 and MoS_2-COOH sheets characteristic for dispersion in water are shown in Figure 2(c). It can be clearly seen that the

characteristic two exciton peaks of MoS_2 and MoS_2-COOH originating from interband exciton transition at the K point, are located at 688 nm (1.80 eV) and 630 nm (1.97 eV), respectively, indicating a pristine 2H poly-type. The two absorption peaks were direct band transitions with energy split from valence band spin-orbit coupling [49, 50].

Figure 2(d) shows the Fourier transformed infrared (FTIR) absorbance spectra of the main peaks of the MoS_2 and MoS_2-COOH films in attenuated total reflection (ATR) mode, which was analyzed to elucidate the properties of various chemical bonds. The absorption bands can be attributed to the -OH bending mode of the water peak at 1628 cm^{-1}, and the C=O stretching vibration peak at 1738 cm^{-1}, respectively. The peaks at 2848 and 2917 cm^{-1} were attributed to the splitting of -CH_2, and the bands peak at 1059 cm^{-1} is attributed to the stretching vibration of C-OH. As for MoS_2, the water bonding peak at 1632 cm^{-1} and O-H stretching broad band center peak at 3327 cm^{-1} can be seen [46, 48, 51]. The pure BSA peaks at 3062 cm^{-1} for amide A (mainly -NH stretching vibration), 1652 cm^{-1} for amide I (mainly C[double bond, length as m-dash]O stretching vibration) and 1531 cm^{-1} for amide II (the coupling of bending vibrations of N-H and stretching vibration of C-N) [52, 53].

3.2 Analysis of XPS spectra characteristic peaks

The functional modification of MoS_2 with carboxyl molecules and the chemical environment of the different atoms were further analyzed using X-ray photoluminescence spectroscopy (XPS). Figure 3 shows the survey spectrum of MoS_2-COOH along with the high-resolution XPS spectra of S 2p, Mo 3d and C 1s characteristic peaks in Figures 3(a)-3(d) for MCA modification [54, 55]. As shown in Figures 3(a), the survey XPS spectrum of the Au/Cys/MoS_2-COOH chip revealed characteristic peaks for Au, Mo, S, C and O. As shown in Figures 3(b), the high resolution XPS spectrum of Mo binding energies showed two peaks at 232.65 and 229.45 eV for MCA modification, which corresponded to Mo $3d_{3/2}$ and Mo $3d_{5/2}$ of Mo^{4+}, respectively. In addition, the XPS spectrum of S 2s showed

peaks at 226.35 eV that corresponded to MCA modification, respectively. A unique difference in the MCA modified method was a small peak near 234.5 eV corresponding to Mo^{6+} [54]. As shown in Figures 3(c), the XPS spectrum of S binding energies showed two peaks at 163.3 and 162.2 eV for MCA modification, respectively. The functional group of the MCA modification in the XPS spectrum of C 1s binding energies showed a prominent peak at 284.95 eV that could be attributed to C-C (21.2%) bonds, while the other peaks at 285.9 and 289.3 eV were due to C-O-C (48.6%) and O-C=O (30.1%) bonds, respectively, as shown in Figure 3(d). In Figure 3(d), it can be seen that the modified carboxyl group of the MCA method had a higher -COOH group content of 30.1%. The success of using MCA method to introduce carboxylic groups into the MoS_2 sheets was confirmed by the XPS analysis as illustrated in Figure 3.

3.3 Analysis of the characteristics of protein immobilization

We used a low volume of 20 μl and different BSA antigen concentrations to carry out the immobilization procedure on the sensing chip. Figure 4(a) shows that the SPR resonance angle shifts of MoS_2-COOH (1 g/l), MoS_2 (1 g/l) and traditional SPR (MOA) chips at a concentration of 2.27 μM BSA were 173.85, 119.78 and 79.83 m°, respectively. From these results, the equilibrium time was determined to be 200 s. The sensitivity of the protein binding ratio analysis was MoS_2-COOH (1 g/l):MoS_2 (1 g/l):conventional chip = 2.2:1.5:1.

We then reduced the BSA protein concentration to 1.52 μM and compared the resonance angular shifts of protein immobilization efficiency on the four chips (Figure 4(b)). The SPR resonance angle shifts of MoS_2-COOH (0.5 g/l), MoS_2 (0.5 g/l) and traditional SPR (MOA) chips at a concentration of 1.52 μM BSA were 78.79, 56.44 and 54.19 m°, respectively. Figures 4(a) and 4(b) present the molecule bonding force of the BSA antigen, revealing a high response of the SPR angle shift to the MCA-modified MoS_2-COOH chip. The sensitivity of the protein binding ratio analysis was MoS_2-COOH (0.5 g/l):MoS_2 (0.5 g/l) =

1.4:1. The experimental results showed that the MCA-modified MoS_2-COOH chip had a larger protein binding ratio.

3.4 SPR immunoassay of bioaffinity interactions

Figure 5 shows real-time SPR sensorgrams comparing the relationship between the antigen-antibody interactions in 20 μl volume and the SPR angular shifts in the five different sensing chips. The SPR sensorgrams were obtained for 14.5, 72.5, 145, 362, 725 and 1450 nM of anti-BSA on the MoS_2-COOH (1 g/l) chip at 4.69, 21.15, 69.62, 107.85, 187.84, and 227.91 m°, as shown in Figure 5(a). Figures 5(a) and 5(b) show the MoS_2-COOH (1 g/l) and MoS_2-COOH (0.5 g/l) chips, we injected different concentrations of antibodies to analyze the resonance angular shifts. The results showed that the MoS_2-COOH (1 g/l) chip clearly reached saturation at 1450 nM, and therefore there were no significant differences in the SPR angle shift of MoS_2-COOH (1 g/l) and MoS_2-COOH (0.5 g/l) chips at other concentrations. In terms of the binding interaction characteristics of the TMD-based sensing chips, the SPR angle shifts were 2.49, 16.82, 48.07, 93.87, 178.28 and 203.56 m° for the MoS_2 chip and 1.23, 6.16, 15.69, 46.83, 86.28 and 117.49 m° for the WS_2 chip. The experimental results showed that the sensitivity of WS_2 was not as high as that of MoS_2, which is consistent with previous studies [56]. Comparisons between the measured angle shifts for the MoS_2-COOH (1 g/l) chip to those of the MoS_2 and WS_2 chips in 14.5 nM of anti-BSA revealed relative 2-fold and 4-fold increases in the SPR angle as shown in Figures 5(a), 5(c) and 5(d). Figures 5(a) and 5(e) show that the ratios of the SPR angle shifts of the MoS_2-COOH (1 g/l) chip to that of the traditional SPR (MOA) chip in 14.5, 72.5, 145, 362, 725 and 1450 nM of anti-BSA were increased by 3.1, 3.0, 3.1, 2.7, 2.5 and 2.3-folds, respectively. In summary, the results clearly showed that the MoS_2-COOH chip had the highest sensitivity compared to the other chips. We analyzed the linear range sensitivity as a series of concentrations in the five different chips. Linear calibration curve fitting showed

the relationship between SPR angle shift and anti-BSA concentrations from 14.5 to 725 nM for the five different sensing chips. The SPR immunosensors for the exponential regression of the linear curve in Figure 5(f) yielded y= 0.43+0.30x and R^2= 0.95 for the MoS_2-COOH (1 g/l) chip, y= -1.13+0.29x and R^2= 0.97 for the MoS_2-COOH (0.5 g/l) chip, y= -1.38+0.27x and R^2= 0.98 for the MoS_2 (1 g/l) chip, y= -0.10+0.11x and R^2= 0.97 for the WS_2 (1 g/l) chip and y= -0.40+0.11x and R^2= 0.97 for the traditional SPR (MOA) chip, where x denotes the refractive concentration and y is the SPR angle. The results clearly indicated that the MoS_2-COOH chip had excellent detection sensitivity. The MoS_2- and WS_2-based sensing chips captured the biomolecules through the van der Waals interaction [37, 40]. The MoS_2 and WS_2 chips yielded an SPR angle shift that was less than that of the MoS_2-COOH chip, which may have been because protein absorption of MoS_2 and WS_2 were not stable and could easily fall off. The high performance of this MoS_2-COOH biosensor (high sensitivity, LOD of 1.45 pM, good regeneration) will allow for the creation of fast, inexpensive and reliable biosensors for applications in clinical medicine and healthcare.

We measured the limit of detection (LOD) of the MoS_2-COOH-based SPR chip for antibody immunoassays at concentrations of 0.145, 1.45, and 145 pM. The experimental results showed a LOD of 1.45 pM within a response time of only 150 s in the MoS_2-COOH-based SPR chip (Figure 6(a)). In molecular kinetic analysis, the SPR sensorgrams of experimental curve-fitting for a simple binding curve showed a 1:1 steady state of the Langmuir model [57]. Association and dissociation rate constants were calculated by nonlinear fitting of the SPR sensorgram data (Figure 6(b)). All binding data were analyzed using biomolecular binding specificity analysis evaluation software version 2.4.4 (Biosensing Instrument, Tempe, AZ, USA). In these different SPR-based immunosensors, the kinetics of protein interaction analysis could be described by the scheme:

$$[\mathrm{Ab}] + [\mathrm{Ag}] \underset{k_d}{\overset{k_a}{\rightleftarrows}} [\mathrm{Ab \cdot Ag}] \quad (1)$$

$$\mathrm{K_A} = \frac{[\mathrm{Ab{\cdot}Ag}]}{[\mathrm{Ab}][\mathrm{Ag}]} = \frac{1}{\mathrm{K_D}} \quad (2)$$

where [Ab] is the analyte antibody of anti-BSA in solution, [Ag] is the antigen of BSA protein immobilized on the chip surface, ([Ab][Ag]) is the free state, and ([Ab·Ag]) is the binding state. In addition, [Ab], [Ag], and [Ab·Ag] are the corresponding molar concentrations. The calculated equilibrium association rate constant (k_a), dissociation rate constant (k_d), and the equilibrium were determined by the dissociation constant $K_D = k_d/k_a$ [58-60]. In the SPR sensorgram, the bimolecular interaction signal began to level off, and the curve gradually reached equilibrium. The equilibrium between the reactions in Eq. (1) and Eq. (2) had then been established. In the reaction, the rates of association and dissociation phase could be described by the following equation:

$$\mathrm{R_T} = \frac{\mathrm{R_{max}C_{[Ab]}}}{\mathrm{K_D + C_{[Ab]}}}\left[1 - \mathrm{e}^{-(\mathrm{k_a C_{[Ab]} + k_d})\mathrm{T}}\right] \quad (3)$$

where R_T is the SPR signal at time (T), $C_{[Ab]}$ is the concentration of the analyte anti-BSA, and R_{max} is the maximum amount of analyte anti-BSA on the chip surface of the BSA interaction reaction. In the dissociation phase, the following equation suggests that the SPR response was not dependent on the analyte concentration, $C_{[Ab]}$. At equilibrium, the Eq. (3) could be simplified as:

$$\mathrm{R_{eq}} = \frac{\mathrm{R_{max}C_{[Ab]}}}{\mathrm{K_D + C_{[Ab]}}} \quad (4)$$

When non-linear regression analyses were performed based on the above equations, the values of k_a and k_d could be deduced. Consequently, the value of K_A, could also be calculated. The affinity could be judged by the association binding constant of the interaction they describe. A higher value of K_A indicated higher affinity and stronger interaction. Affinity analysis of the kinetics binding data was obtained as previously described [61-63] by plotting R_T vs $C_{[Ab]}$, where R_T is the relative response of the

sensorgram at time (T).

Figure 6(b) shows the affinity analysis of the MoS_2-COOH (1 g/l), MoS_2-COOH (0.5 g/l), MoS_2 (1 g/l), WS_2 (1 g/l) and traditional SPR chips. The kinetic fitted values of K_A were 3.9, 4.1, 0.6, 0.29, and 0.003 × 10^8 M^{-1} for the five chips, respectively. Figure 6(c) shows the kinetic fitting statistics results of k_a were 50.4, 20.6, 0.72, 1.7, and 0.238 × 10^5 M^{-1} S^{-1} for the five chips, respectively. In addition, the ratio of the k_a of the MoS_2-COOH (1 g/l): MoS_2:WS_2: traditional SPR chips was 212:3:7.1:1. The fitting values of k_d were 13.0, 5.0, 1.2, 5.9, and 70 × 10^{-3} S^{-1} for the five chips, respectively, and the fitting values of K_D were 2.42, 2.48, 16.67, 3.50, and 29.4 × 10^{-9} M, respectively. Compared with the traditional SPR and MoS_2 chips, the MoS_2-COOH chip exhibited a higher k_a and lower K_D. This demonstrated that the MoS_2-COOH chip was much more sensitive than the traditional SPR and MoS_2 chips.

3 Conclusions

We propose a new type of MCA-modified carboxylated MoS_2 sheet. In the MCA modification, the mechanism involves chlorine atoms occupying sulfur vacancies to form a strong bonding effect. The results showed that the MoS_2 modified carboxylation technique could enhance the sensitivity and bioaffinity, mainly due to improvements in the dielectric of MoS_2-COOH and the SPR energy coupler properties of MoS_2-COOH. In addition, -COOH had a high affinity with the protein and the formation of covalent bond reactions, resulting in an increase in protein binding efficiency. The MoS_2-COOH chip had a 3.1-fold increase in SPR angle response and increased kinetic association rate constant compared to the traditional SPR chip. The MoS_2-COOH (1 g/l) chip exhibited high affinity for protein interactions since the k_a was 212-folds higher than the traditional SPR chip. More importantly, we proved that the only 20 μl of sample was needed, which is of particular

significance in point-of-care tests and rapid diagnostic tests as well as real-time and label-free devices which can allow for an early diagnosis. We believe that this carboxyl modification approach can be very useful in many applications, such as photonics, electronics and biosensor devices. The application of such biosensing devices may be beneficial in detecting clinical diseases in blood samples, small molecule drug screening and drug resistance analysis.

Acknowledgements

The authors would like to thank the Ministry of Science and Technology of the Republic of China, Taiwan, for financially supporting this research under Contract No. MOST 103-2221-E-003-008, MOST 104-2314-B-195-015, MOST 105-2221-E-003-027 and MOST 106-2221-E-003-020. We thank Dr. Yao-Jane Hsu groups for they help in analyzing XPS spectra (National Synchrotron Radiation Research Center, Beamline 09A2 and 24A1).

References:

[1] Q. H. Wang, K. Kalantar-Zadeh, A. Kis, J. N. Coleman, M. S. Strano, Electronics and optoelectronics of two-dimensional transition metal dichalcogenides. Nat. Nanotech. 7 (2012) 699–712.

[2] R. Lv, J. A. Robinson, R.E. Schaak, D. Sun, Y. Sun, T. E. Mallouk, M. Terrones, Transition metal dichalcogenides and beyond: synthesis, properties, and applications of single- and few-layer nanosheets. Acc Chem Res. 48 (2015) 56–64.

[3] A. A. Tedstone, D. J. Lewis, P. O'Brien, Synthesis, properties, and applications of transition metal-doped layered transition metal dichalcogenides. Chem. Mater. 28 (2016) 1965–1974.

[4] M. Nasilowski, B. Mahler, E. Lhuillier, S. Ithurria, B. Dubertret, Two-dimensional colloidal nanocrystals. Chem. Rev. 116 (2016) 10934–10982.

[5] H. Jiang, Electronic band structures of molybdenum and tungsten dichalcogenides by the GW approach. J. Phys. Chem. C 116 (2012) 7664–7671.

[6] V. Podzorov, M. E. Gershenson, High-mobility field-effect transistors based on transition metal dichalcogenides. Appl. Phys. Lett. 84 (2004) 3301.

[7] C. Gong, H. Zhang, W. Wang, L. Colombo, R. M. Wallace, K. Cho, Band alignment of two-dimensional transition metal dichalcogenides: application in tunnel field effect transistors. Appl. Phys. Lett. 103 (2013) 053513.

[8] D. J. Late, B. Liu, H. S. S. R. Matte, V. P. Dravid, C. N. R. Rao, Hysteresis in single-layer MoS2 field effect transistors. ACS Nano 6 (2012) 5635–5641.

[9] S. Ghatak, A. N. Pal, A. Ghosh, Nature of electronic states in atomically thin MoS2 field-effect transistors. ACS Nano 5 (2011) 7707–7712.

[10] J. S. Ross, P. Klement, A. M. Jones, N. J. Ghimire, J. Yan, D. G. Mandrus, T. Taniguchi, K. Watanabe, K. Kitamura, W. Yao, D. H. Cobden, X. Xu, Electrically tunable excitonic light-emitting diodes based on monolayer WSe2 p–n junctions. Nat. Nanotechnology 9 (2014) 268–272.

[11] H. Tributsch, Layer-type transition metal dichalcogenides — a new class of electrodes for electrochemical solar cells. Ber. Bunsen-Ges. Phys. Chem. 81 (1977) 361–369.

[12] K. K. Kam, B. A. Parklnclon, Detailed photocurrent spectroscopy of the semiconducting group VI transition metal dichaicogenldes. J. Phys. Chem. 86 (1982) 463-467.

[13] M. Thomalla, H. Tributsch, Photosensitization of nanostructured TiO2 with WS2 quantum sheets. J. Phys. Chem. B. 110 (2006) 12167–12171.

[14] M. Pumera, A. H. Loo, Layered transition-metal dichalcogenides (MoS2 and WS2) for sensing and biosensing. TrAC-Trend. Anal. Chem. 61 (2014) 49–53.

[15] D. Sarkar, X. Xie, J. Kang, H. Zhang, W. Liu, J. Navarrete, M. Moskovits, K. Banerjee, Functionalization of ttransition metal dichalcogenides with metallic nanoparticles: implications for doping and gas-sensing. Nano Lett. 15 (2015) 2852–2862.

[16] M. L. Brongersma, N. J. Halas, P. Nordlander, Plasmon-induced hot carrier science and technology. Nat. Nanotechnology 10 (2015) 25–34.

[17] A. Boulesbaa, V. E. Babicheva, K. Wang, I. I. Kravchenko, M.-W. Lin, M. Mahjouri-Samani, C. B. Jacobs, A. A. Puretzky, K. Xiao, I. Ivanov, C. M. Rouleau, D. B. Geohegan, Ultrafast dynamics of metal plasmons induced by 2D semiconductor excitons in hybrid nanostructure arrays. ACS Photonics 3 (2016) 2389–2395.

[18] P. Cudazzo, E. Müller, C. Habenicht, M. Gatti, H. Berger, M. Knupfer, A. Rubio, S. Huotari, Negative plasmon dispersion in 2H-NbS2 beyond the charge-density-wave interpretation. New J. Phys. 18 (2016) 103050.

[19] D. V. Tuan, B. Scharf, I. Žutić, H. Dery, Marrying excitons and plasmons in monolayer transition-metal dichalcogenides. arXiv preprint arXiv 1704 (2017) 01981.

[20] T. Low, A. Chaves, J. D. Caldwell, A. Kumar, N. X. Fang, P. Avouris, T. F. Heinz, F. Guinea, L. Martin-Moreno, F. Koppens, Polaritons in layered two-dimensional materials. Nat. Materials 16 (2017) 182–194.

[21] P. Cudazzo, M. Gatti, A. Rubio, Local-field effects on the plasmon dispersion of two-dimensional transition metal dichalcogenides. New J. Phy. 15 (2013) 125005.

[22] Z. Wang, Z. Dong, Y. Gu, Y.-H. Chang, L. Zhang, L.-J. Li, W. Zhao, G. Eda, W. Zhang, G. Grinblat, S. A. Maier, J. K. W. Yang, C.-W. Qiu, A. T. S. Wee, Giant photoluminescence eEnhancement in tungsten-diselenide–gold plasmonic hybrid structures. Nat. Comm. 7 (2016) 11283.

[23] Z. Bao, X. Liu, Y. Liu, H. Liu, K. Zhao, Near-infrared light-responsive inorganic nanomaterials for photothermal therapy. Asian J. Pharm. Sci. 11 (2016) 349-364.

[24] A. Kuc, N. Zibouche, T. Heine, Influence of quantum confinement on the electronic structure of the transition metal sulfide TS_2. Phys. Rev. B 83 (2011) 245213.

[25] S. W. Han, H. Kwon, S. K. Kim, S. Ryu, W. S. Yun, D. H. Kim, J. H. Hwang, J.-S. Kang, J. Baik, H. J. Shin, S. C. Hong, Band-gap transition induced by interlayer van der waals interaction in MoS_2. Phys. Rev. B 84 (2011) 045409.

[26] P. Johari, V.B. Shenoy, Tunable dielectric properties of transition metal dichalcogenides. ACS Nano 5 (2011) 5903–5908.

[27] J. N. Coleman, M. Lotya, A. O'Neill, S. D. Bergin, P. J. King, U. Khan, K. Young, A. Gaucher, S. De, R. J. Smith, I. V. Shvets, S. K. Arora, G. Stanton, H.-Y. Kim, K. Lee, G. T. Kim, G. S. Duesberg, T. Hallam, J. J. Boland, J. J. Wang, J. F. Donegan, J. C. Grunlan, G. Moriarty, A. Shmeliov, R. J. Nicholls, J. M. Perkins, E. M. Grieveson, K. Theuwissen, D. W. McComb, P. D. Nellist, V. Nicolosi, Two-dimensional nanosheets produced by liquid exfoliation of layered materials. Science 331 (2011) 568–571.

[28] B. Mukherjee, N. Kaushik, R. P. N. Tripathi, A. M. Joseph, P. K. Mohapatra, S. Dhar, B. P. Singh, G. V. Pavan Kumar, E. Simsek, S. Lodha, Exciton emission intensity modulation of monolayer MoS2 via Au plasmon coupling. Sci. Rep. 7 (2017) 41175.

[29] Y. Wang, J. Z. Ou, A. F. Chrimes, B. J. Carey, T. Daeneke, M. M. Y. A. Alsaif, M. Mortazavi, S. Zhuiykov, N. Medhekar, M. Bhaskaran, J. R. Friend, M. S. Strano, K. Kalantar-Zadeh, Plasmon resonances of highly doped two-dimensional MoS_2. Nano Lett. 15 (2015) 883–890.

[30] J. Yan, C. Ma, P. Liu, G. Yan, Plasmon-induced energy transfer and photoluminescence manipulation in MoS_2 with a different number of layers. ACS Photonics 4 (2017) 1092–1100.

[31] W. Liu, B. Lee, C. H. Naylor, H.-S. Ee, J. Park, A. T. C. Johnson, R. Agarwal, Strong exciton–plasmon coupling in MoS_2 coupled with plasmonic lattice. Nano Lett. 16 (2016) 1262–1269.

[32] Z. Zhu, J. Yuan, H. Zhou, J. Hu, J. Zhang, C. Wei, F. Yu, S. Chen, Y. Lan, Y. Yang, Y. Wang, C. Niu, Z. Ren, J. Lou, Z. Wang, J. Bao, Excitonic resonant emission−absorption of surface plasmons in transition metal dichalcogenides for chip-level electronic−photonic integrated circuits. ACS Photonics 3 (2016) 869−874.

[33] T. Hong, B. Chamlagain, S. Hu, S. M. Weiss, Z. Zhou, Y.-Q. Xu, Plasmonic hot electron induced photocurrent response at MoS_2–metal junctions, ACS Nano 9 (2015) 5357–5363.

[34] S. Butun, S. Tongay, K. Aydin, Enhanced light emission from large-area monolayer MoS_2 using plasmonic nanodisc arrays. Nano Lett. 15 (2015) 2700–2704.

[35] H. Li, Z. Yin, Q. He, H. Li, X. Huang, G. Lu, D. W. H. Fam, A. I. Y. Tok, Q. Zhang, H. Zhang, Fabrication of single- and multilayer MoS_2 film-based field-effect transistors for sensing NO at room temperature. Small 8 (2012) 63–67.

[36] D. Sarkar, W. Liu, X. Xie, A. C. Anselmo, S. Mitragotri, K. Banerjee, MoS2 field-effect transistor for next-generation label-free biosensors. ACS Nano 8 (2014) 3992–4003.

[37] J. Lee, P. Dak, Y. Lee, H. Park, W. Choi, M. A. Alam, S. Kim, Two-dimensional layered MoS2 biosensors enable highly sensitive detection of biomolecules. Sci. Rep. 4 (2014) 7352.

[38] K. Kalantar-zadeh, J. Z. Ou, Biosensors based on two-dimensional MoS2. ACS Sens. 1 (2016) 5−16.

[39] L. Wang, Y. Wang, J. I. Wong, T. Palacios, J. Kong, H. Y. Yang, Functionalized MoS2 nanosheet-based fField-effect biosensor for label-free sensitive detection of cancer marker proteins in solution. Small 10 (2014) 1101–1105.

[40] Q. Ouyang, S. Zeng, L. Jiang, L. Hong, G. Xu, X.-Q. Dinh, J. Qian, S. He, J. Qu, P. Coquet, K.-T. Yong, Sensitivity enhancement of transition metal dichalcogenides/silicon nanostructure-based surface plasmon resonance biosensor. Sci Rep. 6 (2016) 28190.

[41] S. Zeng, S. Hu, J. Xia, T. Anderson, X.-Q. Dinh, X.-M. Meng, P. Coquet, K.-T. Yong, Graphene–MoS2 hybrid nanostructures enhanced surface plasmon resonance biosensors. Sens. Act. B Chem. 207 (2015) 801–810.

[42] L. Wu, Y. Jia, L. Jiang, J. Guo, X. Dai, Y. Xiang, D. Fan, Sensitivity improved SPR biosensor based on the MoS2/graphene–aluminum hybrid structure. J. Lightw. Technol. 35 (2017) 82-87.

[43] F. OuYang, B. Huang, Z. Li, J. Xiao, H. Wang, H. Xu, Chemical functionalization of graphene nanoribbons by carboxyl groups on stone-wales defects, J. Phys. Chem. C 112 (2008) 12003-12007.

[44] I. Ozaytekin, The effect of carboxylic acid group on conductivity of the aromatic polyazomethines and char composites, Polym. Compos. 35 (2014) 372-380.

[45] N.-F. Chiu, S.-Y. Fan, C.-D. Yang, T.-Y. Huang, Carboxyl-functionalized graphene oxide composites as SPR biosensors with enhanced sensitivity for immunoaffinity detection. Biosens. Bioelectron. 89 (2017) 370–376.

[46] S. Presolski, M. Pumera, Covalent functionalization of MoS_2. Materials Today, 19 (2016) 140–145.

[47] L. Yang, K. Majumdar, H. Liu, Y. Du, H. Wu, M. Hatzistergos, P. Y. Hung, R. Tieckelmann, W. Tsai, C. Hobbs, P. D. Ye, Chloride molecular doping technique on 2D materials: WS_2 and MoS_2. Nano Letters 14 (2014) 6275–6280.

[48] X. Yang, N. Meng, Y. Zhu, Y. Zhou, W. Nie, P. Chen, Greatly improved mechanical and thermal properties of chitosan by carboxyl-functionalized MoS2 nanosheets. J. Mater. Sci. 51 (2016) 1344–1353.

[49] A. K. Mishra, K. V. Lakshmi, L. Huang, Eco-friendly synthesis of metal dichalcogenides nanosheets and their environmental remediation potential driven by visible light, Sci. Rep. 5 (2015) 15718.

[50] Y.-X. Chen, C.-W. Wu, T.-Y. Kuo, Y.-L. Chang, M.-H. Jen, I-W. P. Chen, Large-scale production of large-size atomically thin semiconducting molybdenum dichalcogenide Ssheets in water and its application for supercapacitor, Sci. Rep. 6 (2016) 26660.

[51] K. Zhou, S. Jiang, C. Bao, L. Song, B. Wang, G. Tang, Y. Hu, Z. Gui, Preparation of Poly(vinyl alcohol) nanocomposites with molybdenum disulfide (MoS_2): structural characteristics and markedly enhanced properties, RSC Adv. 2 (2012) 11695–11703.

[52] D. Ghosh, S. Mondal, S. Ghosh, A. Saha, Protein conformation driven biomimetic synthesis of semiconductor nanoparticles, J. Mater. Chem. 22 (2012) 699–706.

[53] P. Huang, Y. Kong, Z. Li, F. Gao, D. Cui, Copper selenide nanosnakes: bovine sSerum albumin-assisted room temperature controllable synthesis and characterization, Nano. Res Lett. 5 (2010) 949–956.

[54] C. Ahn, J. Lee, H.-U. Kim, H. Bark, M. Jeon, G. H. Ryu, Z. Lee, G. Y. Yeom, K. Kim, J. Jung, Y. Kim, C. Lee, T. Kim, Low-temperature synthesis of large-scale molybdenum disulfide thin films directly on a plastic substrate using plasma-enhanced chemical vapor deposition, Adv. Mater. 27 (2015) 5223–5229.

[55] P. K. Rastogi, S. Sarkar, D. Mandler, Ionic strength induced electrodeposition of two-dimensional layered MoS2 nanosheets, App. Mater. Today 8 (2017) 44–53.

[56] Y. Xu, C.-Y. Hsieh, L. Wu, L. K. Ang, Ultrasensitive and highly accurate long-range surface plasmon resonance biosensors based on two-dimensional transition metal dichalcogenides, arXiv:1709.08813.

[57] D. J. Oshannessy, M. Brighamburke, K.K. Soneson, P. Hensley, I. Brooks, Determination of rate and equilibrium binding constants for macromolecular interactions using surface plasmon resonance: use of non-linear least squares analysis methods. Anal. Biochem. 212 (1993) 457–468.

[58] N.-F. Chiu, T.-Y. Huang, Sensitivity and kinetic analysis of graphene oxide-based surface plasmon resonance biosensors. Sens. Act. B Chem. 197 (2014) 35–42.

[59] N.-F. Chiu, T.-Y. Huang, H.-C. Lai, K.-C. Liu, Graphene oxide-based SPR biosensor chip for immunoassay applications. Nanoscale. res. lett. 9 (2014) 445–451.

[60] N.-F. Chiu, C.-T. Kuo, T.-L. Lin, C.-C. Chang, C.-Y. Chen, Ultra-high sensitivity of the non-immunological affinity of graphene oxide-peptide based surface plasmon resonance biosensors to detect human chorionic gonadotropin. Biosens. Bioelectron. 94 (2017) 351–357.

[61] K. Sigmundsson, G. Masson, R. Rice, N. Beauchemin, B. Obrink, Determination of active concentrations and association and dissociation rate constants of interacting biomolecules: an analytical solution to the theory for kinetic and mass transport limitations in biosensor technology and its experimental verification. Biochemistry 41 (2002) 8263–8276.

[62] S. Lin, A. S.-Y. Lee, C.-C. Lin, and C.-K. Lee, Determination of binding constant and stoichiometry for antibody-antigen interaction with surface plasmon resonance. Current Proteomics 3 (2006) 271–282.

[63] D. G. Myszka, Kinetic analysis of macromolecular interactions using surface plasmon resonance biosensors. Curr. Opin. Biotechnol. 8 (1997) 50–57.

Figure 1. Preparation of the MoS_2-COOH-based SPR immunosensor techniques incorporating a protein for the detection of analytes including (a) synthesis methods (b) immobilization procedures and (c) sensing mechanism.

Figure 2. TEM images of the architecture of (a) MoS_2 and (b) MoS_2-COOH sheets. (c) UV-vis absorption spectrum for MoS_2 and MoS_2-COOH dispersion in water. (d) Analysis of FTIR of the monochloroacetic acid (MCA) carboxylated modified MoS_2-COOH, MoS_2 and MoS_2-COOH/BSA chips.

Figure 3. The XPS survey spectra (a) and high resolution XPS spectra of Mo 3d (b), S 2p (c), and C 1s (d) of MoS2-COOH thin films.

Figure 4. Comparison of the efficiency of immobilizing different concentrations of protein on the sensing chips (a) 2.27 μM and (b) 1.52 μM at an injection volume of 20 μl.

Figure 5. SPR sensorgrams of the label-free detection immunoassay during binding reactions between antigen-antibody interactions and sensing interface, showing the angle shift in (a) MoS_2-COOH (1 g/l), (b) MoS_2-COOH (0.5 g/l), (c) MoS_2 (1 g/l) (d) WS_2 (1 g/l) and (e) traditional SPR (MOA) chips. (f) The linear calibration curves of the five different sensing chips in the antigen-antibody interactions of the SPR assay.

Figure 6. (a) The detection limit of the SPR-based MoS_2-COOH biosensor. Kinetic analysis of the five different sensing chips in the antigen-antibody interactions of the SPR assay. (b) The affinity analysis of BSA and anti-BSA protein interactions for SPR sensorgram in

real-time. (c) Molecular kinetic analysis of the interaction factors determining the efficiency of the different chips.

Figure 1.

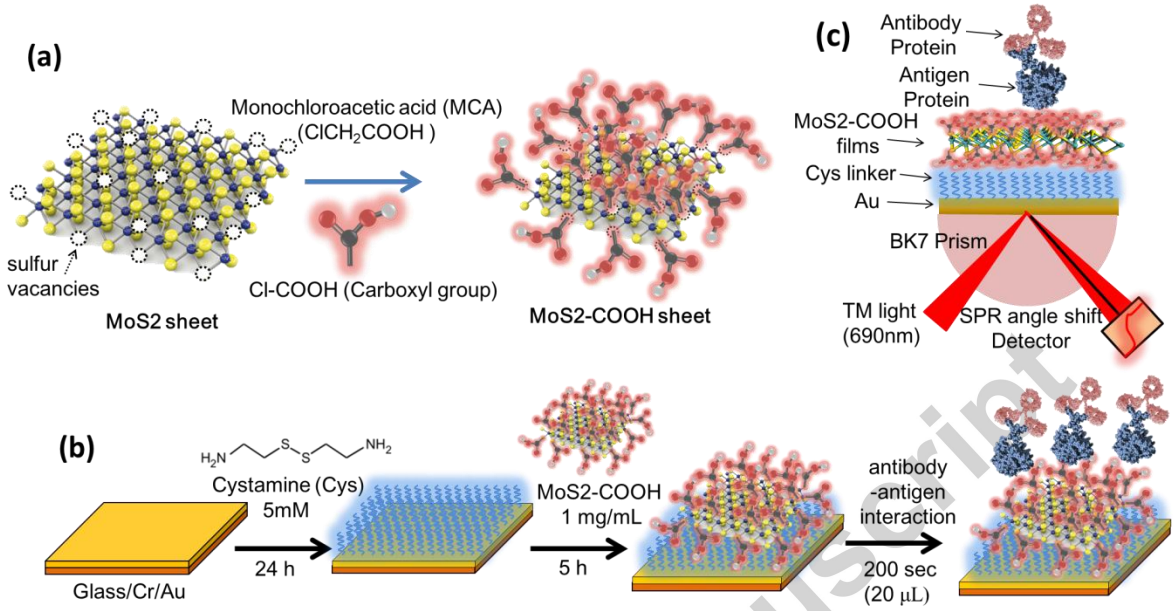

Figure 2.

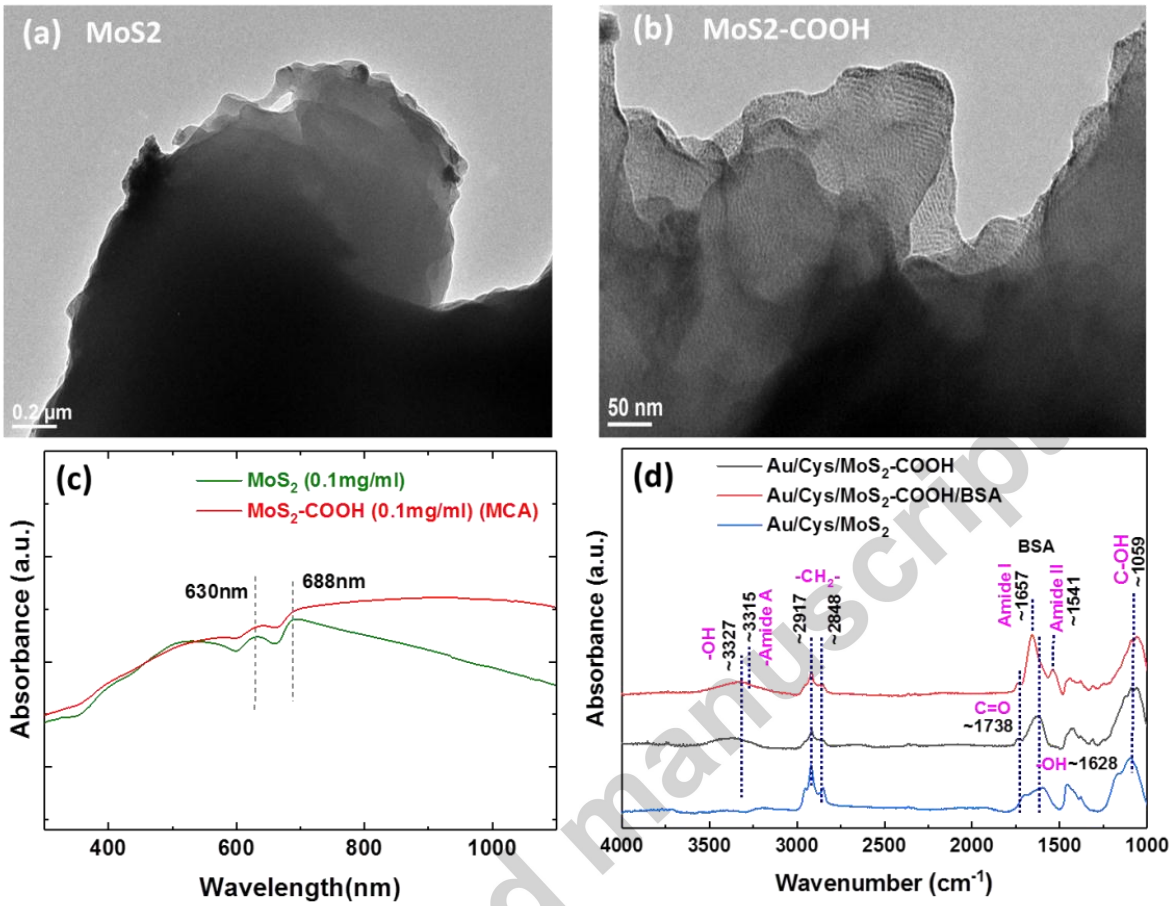

Figure 3.

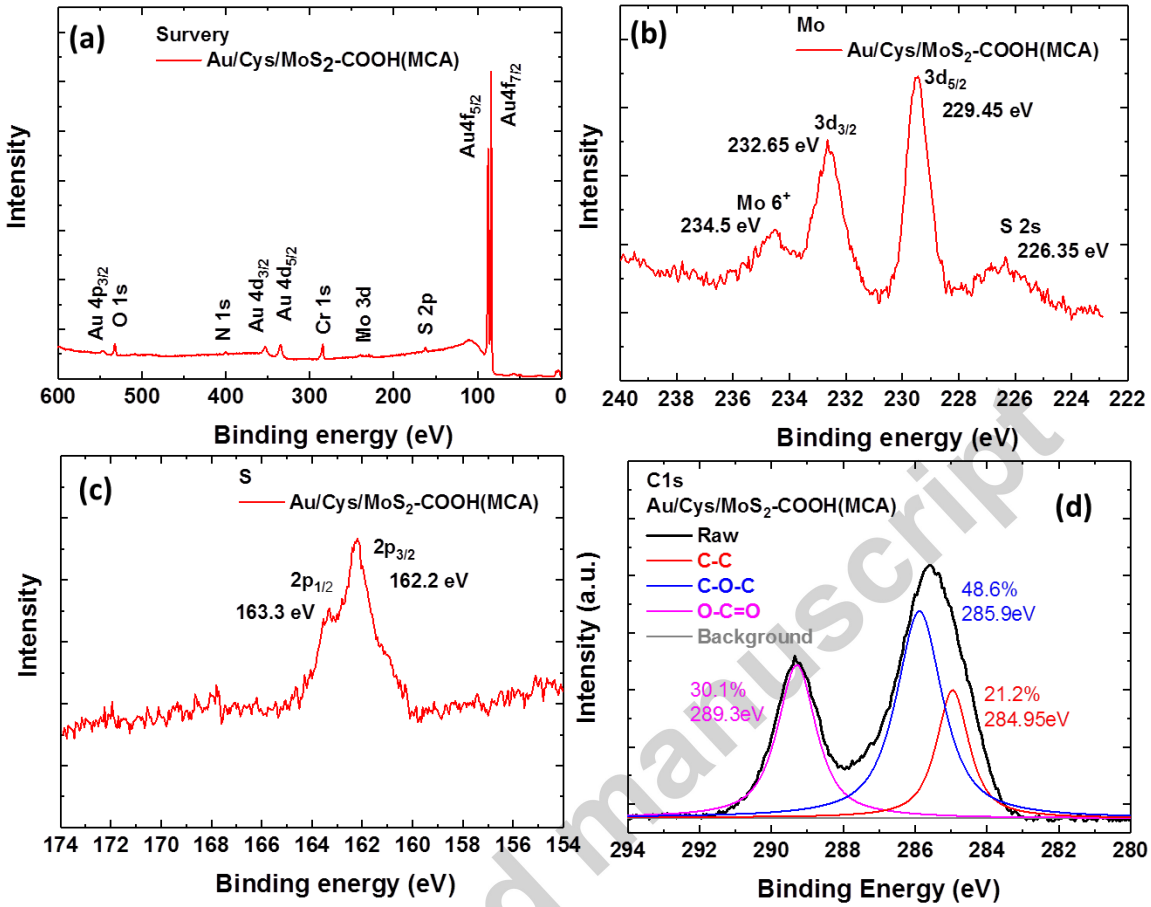

Figure 4.

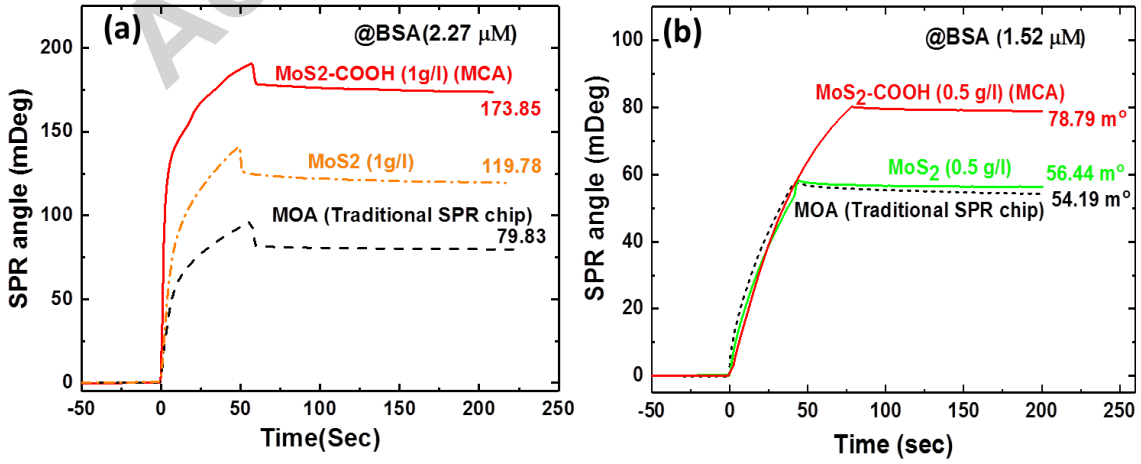

Figure 5.

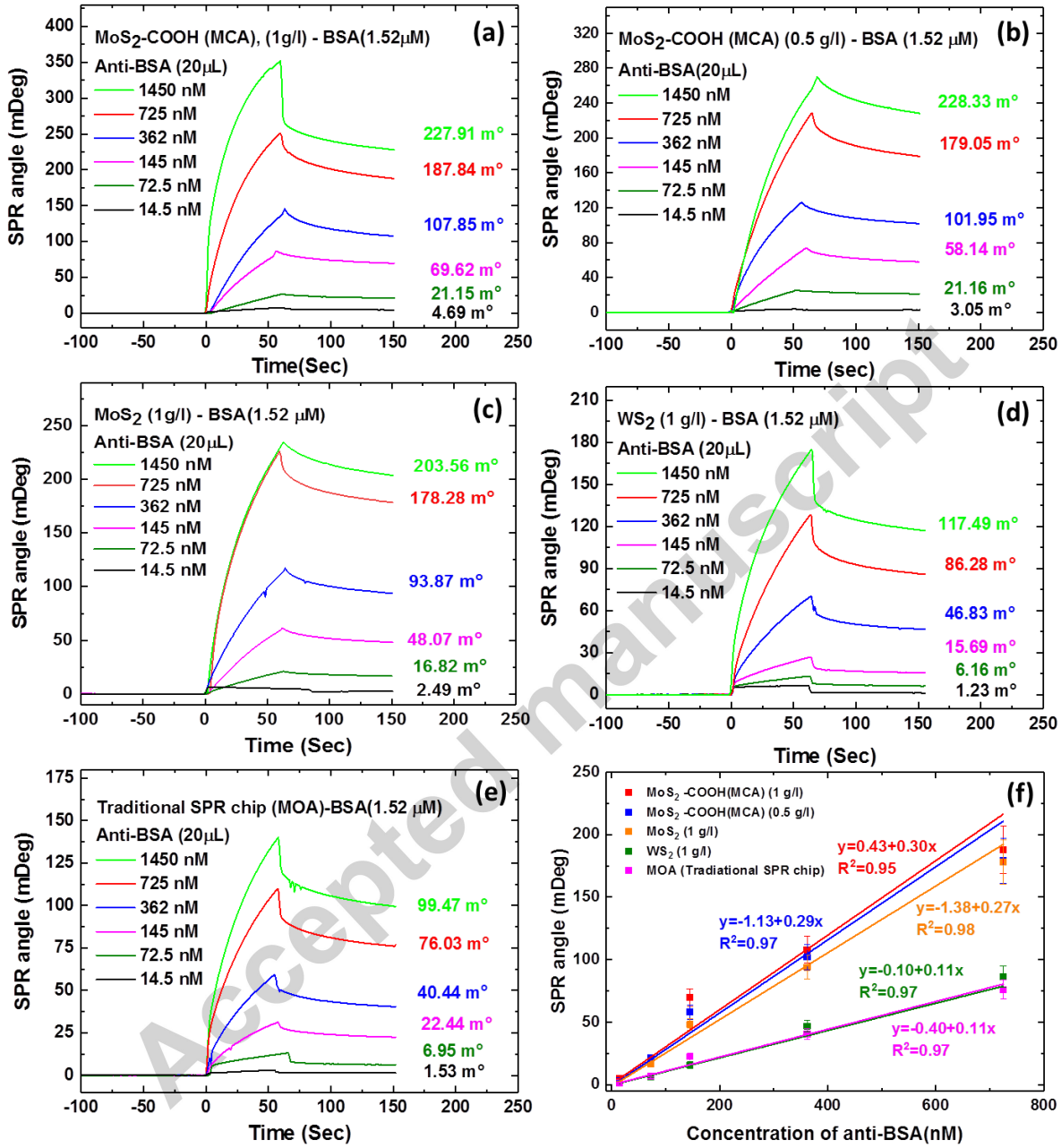

Figure 6.

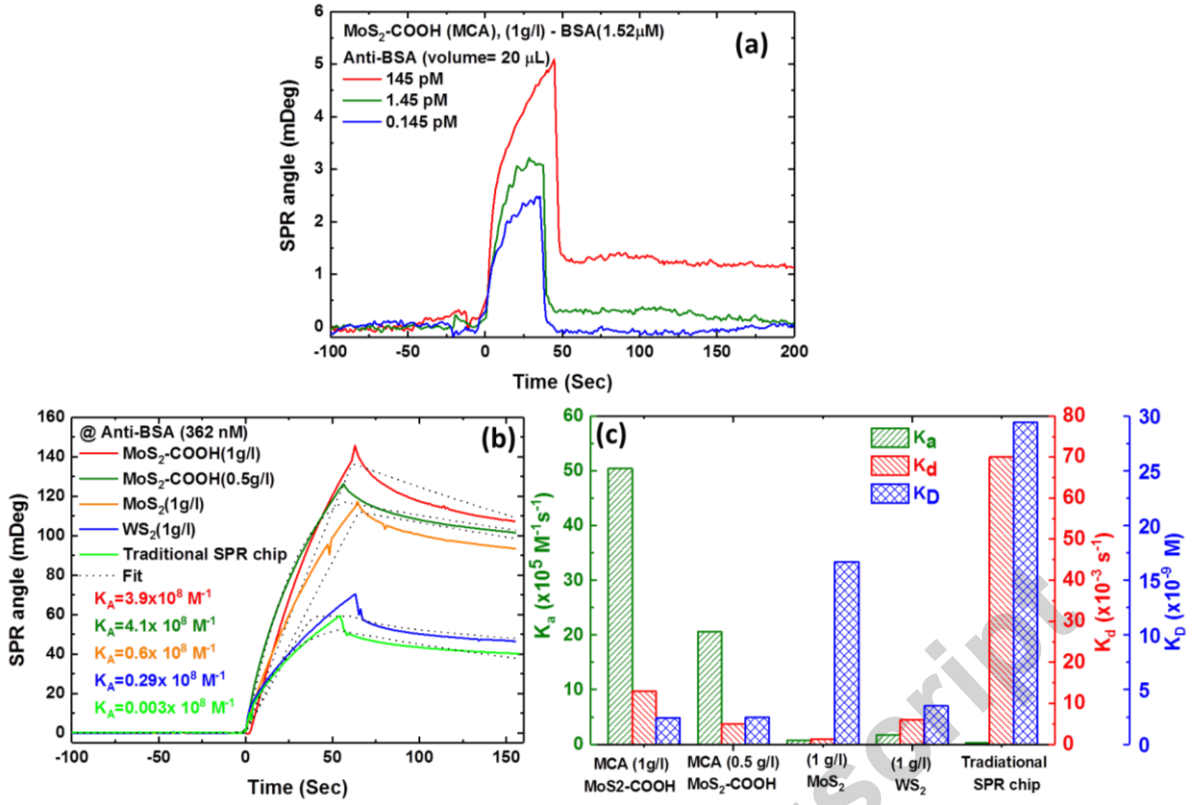

Highlights

- This work demonstrates the excellent potential of SPR-based biosensors to generate MoS_2-COOH as biocompatible surfaces on sensing films.
- The affinity binding of the MoS_2-COOH chip can be significantly enhanced by up to ~6.5 folds that of the MoS_2 chip.
- The MoS_2-COOH chip could amplify the SPR angle response by 3.1 folds and enhance the high association rate of ka by 212 folds compared to MoS_2 and traditional SPR chips.